Обзор ArXiv/astro-ph, 16-23 декабря 2019

От Сильченко О.К.

ArXiv: 1912.08845

Formation of S0s in extreme environments I: clues from kinematics and stellar populations.

Lodovico Coccato[1]⋆, Yara L. Jaffé[2], Arianna Cortesi[3,4], Michael Merrifield[5], Evelyn Johnston[6], Bruno Rodríguez del Pino[7], Boris Haeussler[8], Ana L. Chies-Santos[9], Claudia L. Mendes de Oliveira[3], Yun-Kyeong Sheen[10], Karín Menéndez-Delmestre[4].

[1] *European Southern Observatory, Karl-Schwarzchild-str., 2, 85748 Garching b. München, Germany.*
[2] *Instituto de Física y Astronomía, Facultad de Ciencias, Universidad de Valparaíso, Gran Bretaña 1111, 5030 Casilla, Valparaíso, Chile.*
[3] *Instituto de Astronomia, Geofísica e Ciências Atmosféricas (IAG), Universidade de São Paulo (USP), R. do Matão 1226, 05508-090 São Paulo,*
[4] *Observatorio de Valongo, Universidade Federal do Rio de Janeiro, Ladeira do Pedro Antônio, 43, Centro, Rio de Janeiro - RJ, 20080-090, Bra*
[5] *School of Physics and Astronomy, University of Nottingham, University Park, Nottingham NG7 2RD, UK.*
[6] *Pontificia Universidad Catolica de Chile, Av. Vicuna Mackenna 4860, 7820436 Macul, Santiago, Chile.*
[7] *Centro de Astrobiología (CSIC-INTA), Torrejón de Ardoz, E-28850 Madrid, Spain.*
[8] *European Southern Observatory, Alonso de Cordova 3107 Vitacura Casilla 7630355 Santiago, Chile.*
[9] *Departamento de Astronomia, Universidade Federal do Rio Grande do Sul, Av. Bento Gonçalves 9500, 91501-970 Porto Alegre, RS, Brazil.*
[10] *Korea Astronomy and Space Science Institute, 776, Daedeokdae-ro, Yuseong-gu, Daejeon 34055, Korea.*

GALAXY (1)	Alt. NAME (2)	Sample (3)	Type (4)	Distance [Mpc] (5)	M_K [mag] (6)	M_B [mag] (7)	W1 [mag] (8)	$\log\left(\frac{R_e}{''}\right)$ (9)	$\frac{V_{rot}}{\sigma(R_e)}$ (10)	$\lambda(R_e)$ (11)	Gas (12)	Exposure [s] (13)
field												
PGC 004187	2MIG 131	M	−2.9	106.5 ± 7.5	−24.67 ± 0.16	–	−22.2 ± 0.2	1.508	0.93	0.36	n	670 × 3 (O)
IC 1989	2MIG 445	M	−2.9	157.1 ± 11.1	−25.36 ± 0.16	−21.6 ± 0.3	−22.8 ± 0.2	1.340	0.73	0.28	i	990 × 9 (O) + 90 × 5 (S
NGC 3546	2MIG 1546	M	−2.5	64.0 ± 4.5	−24.25 ± 0.16	–	−21.6 ± 0.2	1.369	2.43	0.60	y	670 × 4 (O)
PGC 045474	2MIG 1814	M	−3.4	93.8 ± 7.2	−24.60 ± 0.17	–	−22.0 ± 0.2	1.218	0.41	0.19	y	550 × 4 (O) + 60 × 2 (S
NGC 2880	2MIG 1275	A^{3D}	−2.6	21.3 ± 1.9	−22.98 ± 0.20	−19.2 ± 0.3	−20.0 ± 0.2	1.312	2.03	0.55	y	–
NGC 3098	2MIG 1374	A^{3D}	−1.5	23.0 ± 1.8	−22.72 ± 0.18	−19.0 ± 0.2	−19.9 ± 0.2	1.013	1.27	0.35	y	–
NGC 6149	UGC 10391	A^{3D}	−2.0	37.2 ± 3.0	−22.60 ± 0.18	–	−19.9 ± 0.2	1.039	1.52	0.52	y	–
NGC 6278	UGC 10656	A^{3D}	−1.8	42.9 ± 3.4	−24.49 ± 0.17	−20.0 ± 0.2	−21.3 ± 0.2	1.149	2.01	0.38	y	–
NGC 6548	NGC4549	A^{3D}	−1.9	22.4 ± 7.2	−23.19 ± 0.72	−19.6 ± 0.8	−19.2 ± 0.7	1.554	2.18	0.36	y	–
NGC 6703	UGC 11356	A^{3D}	−2.8	25.9 ± 2.8	−23.85 ± 0.24	−20.1 ± 0.3	−20.9 ± 0.2	1.485	0.05	0.06	i	–
NGC 6798	2MIG 2649	A^{3D}	−1.9	37.5 ± 2.7	−23.52 ± 0.16	–	−20.7 ± 0.2	1.093	0.75	0.31	y	–
PGC 056772	NSA 073372	A^{3D}	−1.0	39.5 ± 3.2	−22.06 ± 0.18	–	−19.6 ± 0.2	0.982	0.47	0.33	y	–
cluster												
NGC 4696D	CCC 43	M	−2.1	48.7 ± 4.4	−23.91 ± 0.20	−20.0 ± 0.3	−21.4 ± 0.2	1.344	2.37	0.46	n	520 × 4 (O) + 90 × 2 (S
NGC 4706	CCC 122	M	−1.9	48.7 ± 4.3	−24.08 ± 0.19	−20.1 ± 0.3	−21.3 ± 0.2	1.264	2.71	0.62	i	850 × 6 (O) + 80 × 3 (S
PGC 043435	CCC 137	M	−2.1	48.7 ± 4.3	−23.92 ± 0.19	−20.0 ± 0.3	−21.3 ± 0.2	1.179	1.84	0.40	n	520 × 4 (O)
PGC 043466	CCC 158	M	−2.1	48.7 ± 4.3	−23.20 ± 0.20	−19.4 ± 0.3	−20.5 ± 0.2	1.191	1.35	0.42	i	890 × 6 (O)
NGC 4425	VCC 0984	A^{3D}	−0.6	16.5 ± 1.0	−22.09 ± 0.13	−18.5 ± 0.2	−19.0 ± 0.1	1.349	0.98	0.38	n	–
NGC 4429	VCC 1003	A^{3D}	−0.8	16.5 ± 1.0	−24.32 ± 0.13	−20.1 ± 0.1	−19.0 ± 0.1	1.690	1.29	0.40	y	–
NGC 4435	VCC 1030	A^{3D}	−2.1	16.7 ± 1.0	−23.83 ± 0.13	−19.5 ± 0.1	−20.4 ± 0.1	1.371	1.45	0.54	y	–
NGC 4461	VCC 1158	A^{3D}	−0.7	16.5 ± 1.0	−23.08 ± 0.13	−19.1 ± 0.1	−20.00 ± 0.1	1.356	1.65	0.49	n	–
NGC 4503	VCC 1412	A^{3D}	−1.7	16.5 ± 1.0	−23.22 ± 0.13	−19.0 ± 0.2	−20. ± 0.1	1.449	2.12	0.45	n	–

Notes: Columns 1-2: name of the galaxy. Column 3: dataset the galaxy belongs to: M=MUSE dataset, A^{3D}= Atlas^{3D}. Column 4: Morphological type code according to LEDA (http://leda.univ-lyon1.fr/). Columns 5-6: distance and total M_k luminosity. For galaxies in the MUSE sample, magnitudes are from the 2MASS Extended Source Image server (Cluster sample) and from Karachentseva et al. (2010, field sample), distances from NED (NASA/IPAC Extragalactic Database), assuming H_0 = 70 km s^{-1} Mpc^{-1}, Ω_Λ = 0.3, Ω_M = 0.7. For galaxies in the ATLAS 3D sample, magnitudes and distances are as reported in Cappellari et al. (2011a). Error on magnitude includes the contribution from the error on the distance. Column 7: Total apparent "face-on" magnitude corrected for galactic and internal extinction, and for redshift (from de Vaucouleurs et al. 1991). Error on magnitude includes the contribution from the error on the distance. Column 8: WISE (Wright et al. 2010) W1 magnitudes at 3.4 μ, corrected for internal and galactic extinction, and with aperture and k corrections (Sorce et al. 2012). Error on magnitude includes the contribution from the error on the distance. Column 9: $\log_{10}$ of the effective radius. For galaxies in the MUSE sample, the value is fitted with `galfit` (Peng et al. 2002) on the reconstructed image obtained from the datacubes its associated error is ~ 10%. For the ATLAS 3D sample the value of R_e is as reported by Cappellari et al. (2013), its associated error is ≈ 22% according to Section 4.1 of Cappellari et al. (2013). Columns 10 and 11: values of V_{rot}/σ and the λ parameter within 1 effective radius

8 галактик - MUSE, 13 - SAURON

Результаты анализа полных полей скоростей

Table 2. Best fit parameters of the kinemetry and Jeans axisimmetric models.

GALAXY (1)	$\langle PA_{\rm KIN}\rangle$ (2)	$\langle q\rangle$ (3)	$V_{\rm circ}$ [km s^{-1}] (4)	$M_{\rm star}$ [$M_\odot/10^{10}$] (5)	$M/L_{\rm star}$ (6)	$Incl$ [deg] (7)	β (8)	$M_{\rm DM}$ [$M_\odot/10^{10}$] (9)	r_s [pc] (10)	D/T (11)
field										
PGC 004187	121.7 ± 0.4	0.44 ± 0.05	–	28.92 ±11.8	7.14±0.04	90	0.09±0.01	–	–	0.49
IC 1989	136.5 ± 0.4	0.59 ± 0.07	–	37.64 ±15.70	5.53±0.42	90	0.13±0.03	6.00 ± 1.28	2009±11	0.76
NGC 3546	100.0 ± 0.4	0.73 ± 0.11	262± 26	13.47 ±0.40	5.34±0.03	90	0.09±0.01	81.39 ± 0.76	20007±40	0.56
PGC 045474	141.9 ± 0.9	0.62 ± 0.08	271± 27	17.52 ±2.46	5.00±0.14	90	0.16±0.03	10.42 ± 1.28	2000±13	0.63
NGC 2880	142.8 ± 0.6	0.71 ± 0.10	201± 20	3.70 ±0.12	4.28±0.03	51	−0.09±0.03	–	–	0.62$^{(**)}$
NGC 3098	269.9 ± 1.0	0.50 ± 0.06	193± 19	3.19 ±0.11	4.89±0.03	90	0.18±0.01	–	–	0.94
NGC 6149	200.2 ± 0.5	0.71 ± 0.10	147± 15	2.43 ±0.06	4.11±0.03	66	0.01±0.02	–	–	0.73
NGC 6278	306.5 ± 0.2	0.56 ± 0.07	268± 27	10.41 ±0.29	5.43±0.03	66	0.13±0.01	–	–	0.66
NGC 6548	63.1 ± 0.5	0.47 ± 0.05	234± 23	7.27 ±0.44	7.25±0.06	19	−0.96±0.39	–	–	1.00$^{(**)}$
NGC 6703	125.7 ±25.6	0.38 ± 0.04	263± 26	9.40 ±0.07	5.92±0.01	19	−0.08±0.02	–	–	0.53$^{(**)}$
NGC 6798	138.5 ± 1.1	0.28 ± 0.03	191± 19	4.58 ±0.12	4.29±0.03	84	0.09±0.01	–	–	0.50
PGC 056772	190.9 ±26.6	0.40 ± 0.04	129± 13	1.64 ±0.04	3.91±0.03	64	0.46±0.01	–	–	0.37$^{(**)}$
cluster										
NGC 4696D	318.4 ± 0.4	0.44 ± 0.05	–	9.06 ±0.38	5.37±0.04	90	0.07±0.01	–	–	0.44
NGC 4706	27.7 ± 0.2	0.48 ± 0.06	205± 21	7.60 ±0.25	4.81±0.03	90	−0.03±0.01	–	–	0.52
PGC 043435	13.2 ± 0.3	0.52 ± 0.06	–	8.25 ±0.47	6.93±0.06	90	0.05±0.01	–	–	1.00
PGC 043466	325.7 ± 0.4	0.43 ± 0.05	–	4.23 ±0.60	5.00±0.14	90	0.00±0.02	–	–	0.45
NGC 4425	207.0 ± 0.3	0.38 ± 0.04	117± 12	1.66 ±0.01	4.05±0.01	90	0.30±0.00	–	–	0.85$^{(**)}$
NGC 4429	85.3 ± 1.3	0.68 ± 0.09	283± 28	14.70 ±3.05	6.14±0.21	70	0.00±0.01	–	–	0.82$^{(*)}$
NGC 4435	192.8 ± 0.6	0.45 ± 0.05	237± 24	4.88 ±0.27	3.91±0.06	68	0.00±0.02	–	–	0.83
NGC 4461	12.1 ± 0.5	0.57 ± 0.07	190± 19	3.20 ±0.08	3.93±0.02	71	0.12±0.01	–	–	0.69$^{(**)}$
NGC 4503	182.5 ± 0.8	0.70 ± 0.10	208± 21	4.57 ±0.13	5.07±0.03	67	0.24±0.01	–	–	0.68$^{(**)}$

Честно говоря, лажа…

NGC 6798

И тем не менее, нашли разницу динамики S0 в поле и в скоплениях

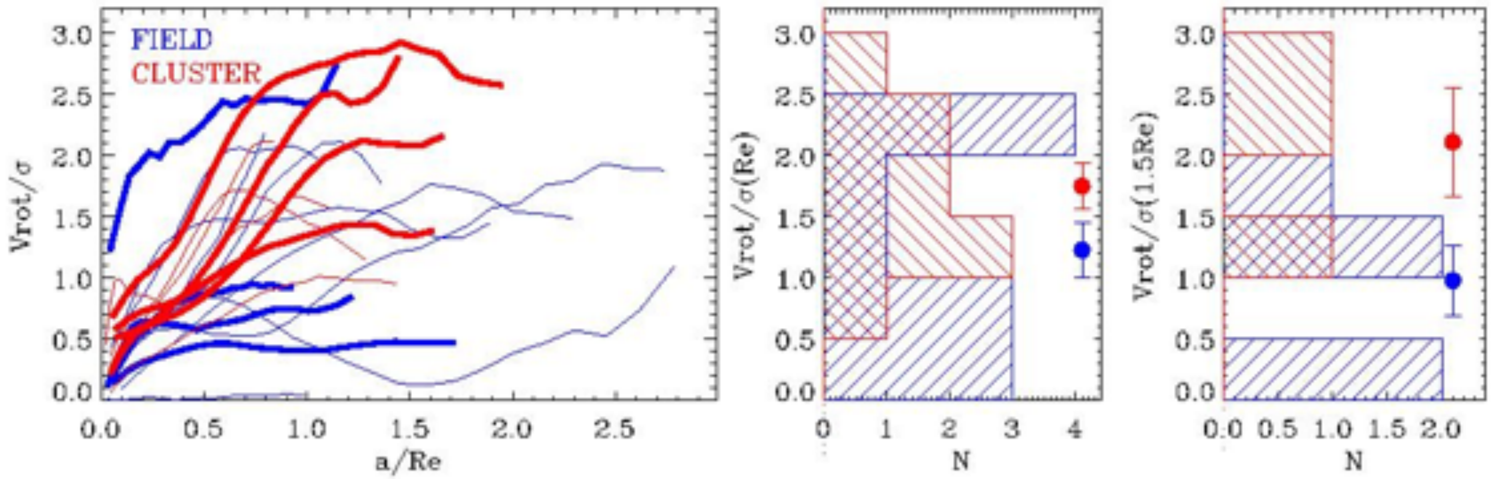

Figure 2. Comparison between the V_{rot}/σ radial profiles of field (blue) and cluster (red) galaxies in our sample. Thick lines identify the MUSE sample, thin lines the ATLAS3D sample. The right-hand side of the figure shows the histograms of the value of V_{rot}/σ at 1 R_e and $1.5R_e$.

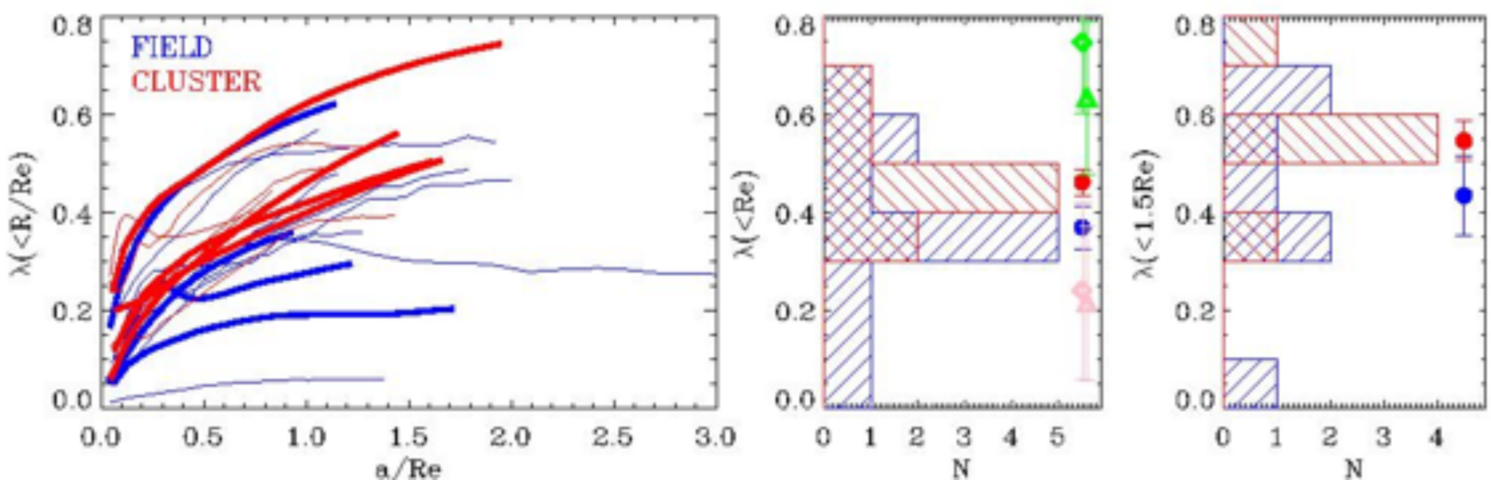

Tully-Fisher

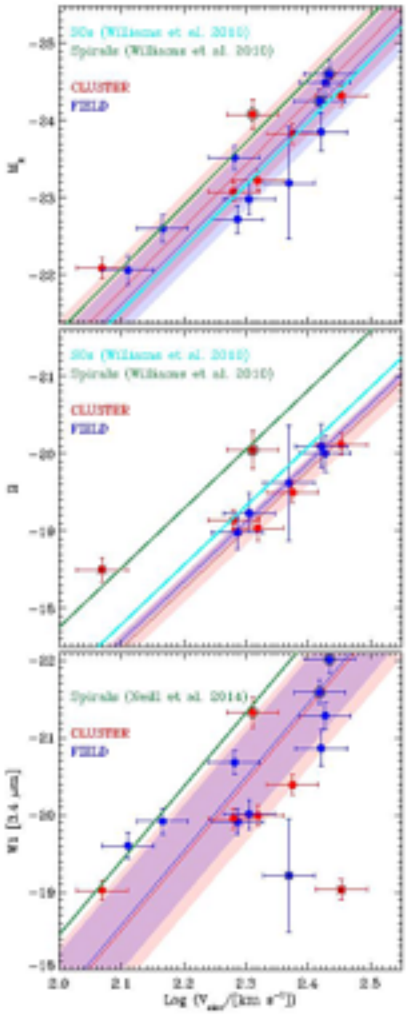

Figure 4. Tully-Fisher relation between circular velocity as determined by Jeans axisymmetric models and K-band (upper panel), B-band (middle panel), and 3.6 μm (lower panel) for field (blue) and cluster (red) galaxies. The thick blue and red lines show the linear fit to the data; shaded area indicate the 1-σ error of the fit. The slope of the S0 Tully-Fisher relation is fixed to the one determined for the Spirals, whose reference is given in each panel. MUSE data are identified by a black circle. As comparison, the Tully-Fisher relations for spirals (green) and S0s (cyan) from Williams et al. (2010) and Neill et al. (2014) are shown. Outliers are identified with crosses in the plots and removed from the fit.

- Подтвеждается сдвиг S0 вниз на зависимости Tully-Fisher…
- И дается совершенно неверная его интерпретация

Разницу в звездных населениях не нашли, а все потому, что внутри эффективного радиуса